International Journal of Solids and Structures 49 (2012) 1712–1722

Contents lists available at SciVerse ScienceDirect

International Journal of Solids and Structures

journal homepage: www.elsevier.com/locate/ijsolstr

Planar mobility modes of 8-bar-jointed structures with a single degree of freedom

H. Tanaka [a,*], Y. Shibutani [b], S. Izumi [a], S. Sakai [a]

[a] Department of Mechanical Engineering, The University of Tokyo, 7-3-1 Hongo, Bunkyo-ku, Tokyo 113-8656, Japan
[b] Department of Mechanical Engineering, Osaka University, 2-1 Yamadaoka, Suita, Osaka 565-0871, Japan

ARTICLE INFO

Article history:
Received 25 March 2011
Received in revised form 13 December 2011
Available online 27 March 2012

Keywords:
Spatial structure
Joint rotation
Planar mobility
Mechanism
Repetitive assembly
Deployable and foldable motions

ABSTRACT

A range of modes of mobility for spatial structures can be achieved by selecting the rotational features of the joints. Similar mechanical characteristics are observed in structures ranging from molecules to buildings. The local rotational manner in a solid with an internal spatial structure performs a key part in dictating the nature of structural deformability. In this paper, we propose a two-dimensional repetitive motion structure assembled with straight rigid bars connected by 8-bar pivot joints. By determining the rotational modes of the 8-bar joint with certain geometrical constraints, we introduce some telescopic transformations of the proposed structure producing both well-known and novel motions. In addition, we verify one of the deployable mechanisms by manufacturing it and testing activation by a single rotary operation.

1. Introduction

Specific spatial structures vary in scale from the cellular to architectural, forming lightweight constructions in limited space capable of resisting external loads or accommodating a wide variety of large deformations (Ashby, 1992; Gibson and Ashby, 1997). Regardless of scale, these spatial structures are made up of connected beam members whose geometrical configuration determines the mode of deformability. Generally the deformation modes can be classified into two groups: stretching dominated structures or bending dominated structures (Deshpande et al., 2001; Wicks and Guest, 2004).

The rotational mechanics of the connections is the key factor in determining the nature of the structural deformability. Some types of bending dominated structures deform because of the coordinated rotation between the beam members through each connection, a mode that can be identified by the co-rotation of each joint. For instance, the functional structures with a negative Poisson's ratio have notable geometrical configurations composed of some specific connections (Evans and Alderson, 2000), which expand laterally when stretched. This type of curious deformation is termed *auxetic behaviour* by Evans et al. (1991). It has been reported that some auxetic behaviours can be achieved by the co-rotation of the rigid components (Smith et al., 2000; Grima and Evans, 2000; Gaspar et al., 2005), where the rotations play a significant role in the structural behaviour.

Our recent work focused on the joint rotation of planar repetitive structures to establish the relationship between overall deformability and the local rotation of planar structures. In addition, we have presented some noteworthy modes of deformation, such as auxetic deformation with a negative Poisson's ratio of a 4-bar jointed structure (Tanaka and Shibutani, 2009), or post-buckling behaviour, with high-energy absorption, of square cells (Tanaka and Shibutani, 2008). These observed mechanical characteristics depend strongly on the flexibility of the joints forming the structure.

Motion structures of the type introduced by You (2007) are spatial structures characterized as movable assemblies according to the rotation of the rigid struts and the rotational interactions of the joints. The applications of the unique deformability of these structures range from exotic toys such as Chuck Hoberman's products (Hoberman Designs Inc., 2011) to satellite solar panels. The most common types of motion structures are scissor-hinge structures (Akgün et al., 2010), and the most basic type is fabricated by assembling straight rigid bars with three pivot joints, one on each end and one in the middle, as shown in Fig. 1(a). All of the joints in this assembly have counter-rotation (relative rotation) motion with a single rotational degree of freedom, and when assembled in a linear fashion, the result is a structure with deployable motion and one kinematical degree of freedom. Fig. 1(b) also illustrates repetitive structures exhibiting a similar deployable motion with counter-rotating joints in a rhombic grid. The extended

* Corresponding author. Tel.: +81 (3) 5841 6412; fax: +81 (3) 3818 0835.
E-mail address: tanaka.hiro@fml.t.u-tokyo.ac.jp (H. Tanaka).

0020-7683/$ - see front matter © 2012 Elsevier Ltd. All rights reserved.
http://dx.doi.org/10.1016/j.ijsolstr.2012.03.008

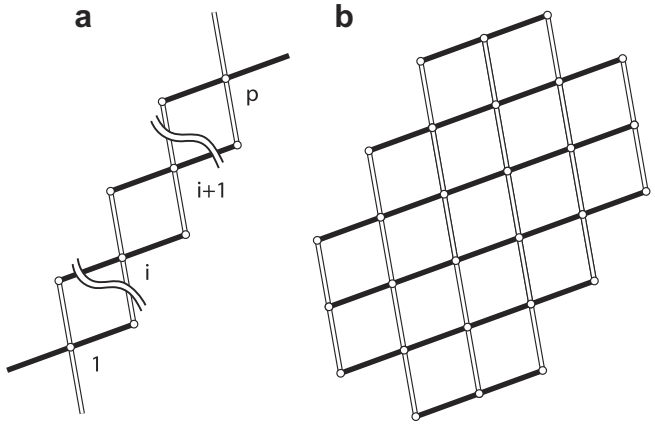

Fig. 1. The most common types of scissor-hinge structures: (a) linear assembly with a mechanism ($m = 1$); (b) repetitive assembly on a rhombic grid, with an overconstrained mechanism.

implementation of the scissor-hinge structure with angulated bars has been proposed by Hoberman (1990), and some novel designs and applications have been proposed: e.g., foldable bar structures with advanced angulated bars (You, 1997; Patel and Ananthasuresh, 2007) and practical retractable roof frameworks (Hoberman, 1991; Buhl et al., 2004). In addition to the regular scissor-hinge structure, all of these structures with angulated bars can achieve their particular folding and expanding motions by counter-rotation of joints arranged in a circular pattern.

The mobility of motion structures is determined by the classic mobility rules attributed to Hunt (1978) to Grübler (1917) or Kutzbach (1929), and by the extended mobility rule of Guest and Fowler (2005). For instance, the Kutzbach criterion has the following form for two-dimensional mechanisms:

$$m = 3(n-1) - 2j_1 - j_2, \tag{1}$$

where m is the mobility of the mechanism, n is the number of links, and j_i is the number of joints having i degrees of freedom. In the case of the scissor-hinge structure in Fig. 1(a), Eq. (1) gives $m = 1$ from $n = 2p$ and $j_1 = p + 2(p-1)$, where p is the number of central pivot joints. However, the repetitive scissor-hinge structure in Fig. 1(b) leads to mobility even though m is negative, which is called an overconstrained mechanism.

It is apparent from the mobility criterion that non-loop movable structures made up of rigid bars connected by joints form a mechanism that behaves as a counter-rotation with a single degree of freedom. However, the mobility of a loop movable structure constructed from the same component set is not always judged by the mobility criterion, because the loop assemblies may be overconstrained. In our study, we determine the detailed structural mobility from the standpoint of the geometric arrangement of the joint rotations.

This paper consists of two parts. We first present the loop structure assembled from 8-bar joints and show that it is valid to predict the possible modes of mobility of the proposed repetitive assembly by examining the rotational modes of the 8-bar joint. In the second part, to verify the obtained mobility, we make the deployable mechanism using a single actuation.

2. Structural model

2.1. Basic structural unit (4RE-linkage)

As shown in Fig. 2(a), the loop structure is made of sixteen identical straight bars connected by eight 2-bar joints and four 4-bar joints, which becomes the elementary unit of the proposed structure discussed in Section 2.2. All the 2-bar joints (unfilled circles) indicate the pinned joint on which the two connected bars can rotate freely. In contrast, we denote the connected states of all the 4-bar joints (grayish circles) as being indefinite. The basic structural unit is a closed-loop with four pairs of rhombic elements (REs) that are incrementally rotated by 90°. We call this structural unit the "4RE-linkage". The initial configurations are determined by the length ℓ and the angle α of the component bars, that is, $\overline{AB} = \overline{BC} = \overline{CD} = \overline{DA} = \ell$, and $\angle ABC = \angle CDA = 2\alpha$, using the symbols in Fig. 2(b).

To understand the mechanism of a 4RE-linkage, let us first review the motions of a single RE framing a 4RE-linkage. Fig. 2(b) illustrates the RE, and the four rigid bars are hinged at A, B, C, and D, indicated by the unfilled circles. The parameters of the planar motion can be described by $\boldsymbol{\theta} = \{\theta_A \theta_B \theta_C \theta_D\}$, where θ_i stands for the respective rotation of each bar. It is clear that we obtain $m = 1$ for the RE as a well-known result for a two-dimensional "four-bar chain" (Calladine, 1978). Compared with the mobility criterion, more detailed motions can be derived from the following condition of a geometrical constraint. Because of the closed-loop configuration, the RE satisfies $\vec{AB} + \vec{BC} + \vec{CD} + \vec{DA} = \mathbf{0}$ for the arbitrary

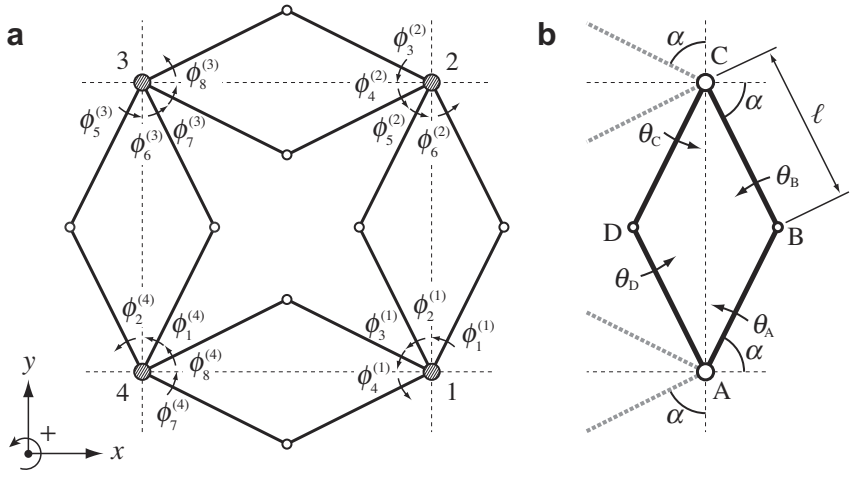

Fig. 2. (a) Structural loop unit (4RE-linkage) is formed by 16 equilateral and rectilinear bars, both ends of which are connected to one another by eight pivots of 2-bar joints (unfilled circles) or four nodes of 4-bar joints (grayish circles) with indefinite bonding; (b) a rhombic element (RE) of a 4RE-linkage.

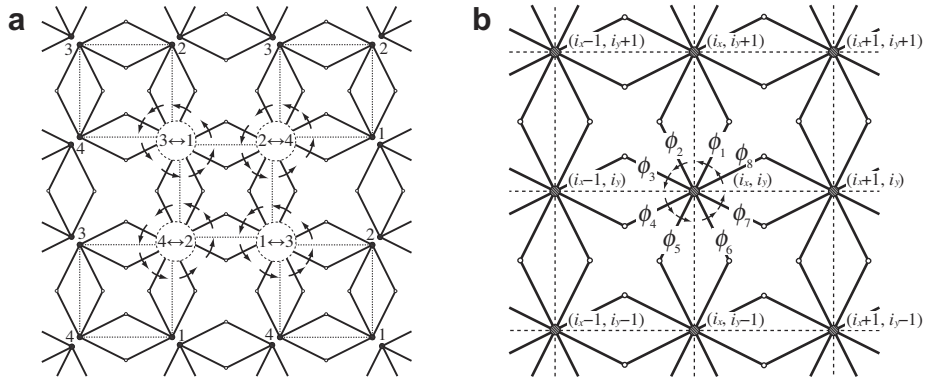

Fig. 3. (a) Repetitive assembly of 4RE-linkages; (b) the rotational parameters of the repetitive structure.

set of rotation parameters $\boldsymbol{\theta}$. Then, it can be rewritten as two component equations with respect to the horizontal and vertical axes (x- and y-axes), as follows:

$$\begin{aligned} &x: \ell\cos(\theta_A+\alpha)+\ell\cos(\theta_B-\alpha+\pi)+\ell\cos(\theta_C+\alpha+\pi)+\ell\cos(\theta_D-\alpha)=0,\\ &y: \ell\sin(\theta_A+\alpha)+\ell\sin(\theta_B-\alpha+\pi)+\ell\sin(\theta_C+\alpha+\pi)+\ell\sin(\theta_D-\alpha)=0. \end{aligned} \tag{2}$$

Arranging Eq. (2) by α, they become

$$\begin{aligned} &x: \cos\alpha(\cos\theta_A-\cos\theta_B-\cos\theta_C+\cos\theta_D)+\sin\alpha(-\sin\theta_A-\sin\theta_B+\sin\theta_C+\sin\theta_D)=0,\\ &y: \cos\alpha(\sin\theta_A-\sin\theta_B-\sin\theta_C+\sin\theta_D)+\sin\alpha(\cos\theta_A+\cos\theta_B-\cos\theta_C-\cos\theta_D)=0. \end{aligned} \tag{3}$$

From Eq. (3), we obtain the following condition of rotations for α in $[0, \pi/2]$:

$$\begin{cases} \theta_A=\theta_C, \theta_B=\theta_D, & \forall\alpha,\\ \theta_A+\theta_D=\theta_B+\theta_C, & \alpha=0,\\ \theta_A+\theta_B=\theta_C+\theta_D, & \alpha=\pi/2. \end{cases} \tag{4}$$

If we assume that all the rotation parameters should be either +1 or −1 because of the coordinated motion with a single degree of freedom for the RE, we obtain four combinations of rotational modes from Eq. (4), as follows:

$$\begin{aligned} &\boldsymbol{\theta}_0=\{+1+1+1+1\}, \forall\alpha,\\ &\boldsymbol{\theta}_1=\{+1-1+1-1\}, \forall\alpha,\\ &\boldsymbol{\theta}_2=\{+1+1-1-1\}, \alpha=0,\\ &\boldsymbol{\theta}_3=\{+1-1-1+1\}, \alpha=\pi/2, \end{aligned} \tag{5}$$

with θ_A selected as +1. In Eq. (5), the rhombic element results in two motions of $\boldsymbol{\theta}_0$ and $\boldsymbol{\theta}_1$ for the arbitrary α. Here, $\boldsymbol{\theta}_0$ indicates the rotation of the overall structure. This overall rotation should be considered to be separate from the other motions accompanied by structural changes. Meanwhile, $\boldsymbol{\theta}_1$ shows the change of rhombic shape corresponding to the action of the mechanism, i.e., $m=1$. In addition, in certain configurations two different types of motion are possible, that is at $\alpha=0$ or at $\alpha=\pi/2$. Thus, the secondary motion exists against the primary motion of $\boldsymbol{\theta}_1$, which is the rotational mode of $\boldsymbol{\theta}_2$ $(\alpha=0)$ or $\boldsymbol{\theta}_3$ $(\alpha=\pi/2)$. Therefore, the configurations for $\alpha=0$ and $\pi/2$ satisfy the condition $m=2$, and these points of intersection of the two different paths, $\{\boldsymbol{\theta}_1, \boldsymbol{\theta}_2\}$ or $\{\boldsymbol{\theta}_1, \boldsymbol{\theta}_3\}$, are called *kinematic bifurcation points* by Kumar and Pellegrino (2000), Tarnai (2001) and Lengyel (2002).

In a similar fashion, we determine the possible motions of a 4RE-linkage. As mentioned above, the primary motions of the rhombic element without a kinematic bifurcation point are the two rotational modes of $\boldsymbol{\theta}_0$ and $\boldsymbol{\theta}_1$. These two motions can be represented by the transformation of the segment AC (the broken line in Fig. 2(b)): $\boldsymbol{\theta}_0$ is the rotation and $\boldsymbol{\theta}_1$ is the elongation and contraction of the segment AC. The segment transformation is determined by two parameters, θ_A and θ_B, because of the constraint of Eq. (4). To take the segment transformation into account, we have the relational expression regarding the movable shape of a 4RE-linkage under the following loop conformation with respect to the x- and y-axes:

$$\begin{aligned} x: &h\left(\frac{\phi_1^{(1)}-\phi_2^{(1)}}{2}\right)\cos\left(\frac{\phi_1^{(1)}+\phi_2^{(1)}}{2}+\frac{\pi}{2}\right)\\ &+h\left(\frac{\phi_3^{(2)}-\phi_4^{(2)}}{2}\right)\cos\left(\frac{\phi_3^{(2)}+\phi_4^{(2)}}{2}+\pi\right)\\ &+h\left(\frac{\phi_5^{(3)}-\phi_6^{(3)}}{2}\right)\cos\left(\frac{\phi_5^{(3)}+\phi_6^{(3)}}{2}+\frac{3\pi}{2}\right)\\ &+h\left(\frac{\phi_7^{(4)}-\phi_8^{(4)}}{2}\right)\cos\left(\frac{\phi_7^{(4)}+\phi_8^{(4)}}{2}\right)=0,\\ y: &h\left(\frac{\phi_1^{(1)}-\phi_2^{(1)}}{2}\right)\sin\left(\frac{\phi_1^{(1)}+\phi_2^{(1)}}{2}+\frac{\pi}{2}\right)\\ &+h\left(\frac{\phi_3^{(2)}-\phi_4^{(2)}}{2}\right)\sin\left(\frac{\phi_3^{(2)}+\phi_4^{(2)}}{2}+\pi\right)\\ &+h\left(\frac{\phi_5^{(3)}-\phi_6^{(3)}}{2}\right)\sin\left(\frac{\phi_5^{(3)}+\phi_6^{(3)}}{2}+\frac{3\pi}{2}\right)\\ &+h\left(\frac{\phi_7^{(4)}-\phi_8^{(4)}}{2}\right)\sin\left(\frac{\phi_7^{(4)}+\phi_8^{(4)}}{2}\right)=0, \end{aligned} \tag{6}$$

where the function h indicates the length of the segment AC and is given by

$$h(t)=2\ell\sin(\alpha+t). \tag{7}$$

In Eq. (6), the two coefficients of each term depend on the parameter $\phi_j^{(i)}$, which represents the rotational displacement of the jth bar on the ith joint as shown in Fig. 2(a). For example, in the first term of the upper Eq. (6), $h(\bullet)$ changes whereas $\cos(\bullet)$ is constant if $\phi_1^{(1)}=-\phi_2^{(1)}$, and vice versa if $\phi_1^{(1)}=\phi_2^{(1)}$. Consequently, Eq. (6) means that each one of the four segments framing a 4RE-linkage must act on either a rotation or an elongation/contraction to retain conformation of a closed-loop. Arranging Eq. (6) in terms of α, they become

$$\begin{aligned} x: &\sin\alpha(-\sin\phi_1^{(1)}-\sin\phi_2^{(1)}-\cos\phi_3^{(2)}-\cos\phi_4^{(2)}+\sin\phi_5^{(3)}+\sin\phi_6^{(3)}\\ &+\cos\phi_7^{(4)}+\cos\phi_8^{(4)})+\cos\alpha(+\cos\phi_1^{(1)}-\cos\phi_2^{(1)}-\sin\phi_3^{(2)}\\ &+\sin\phi_4^{(2)}-\cos\phi_5^{(3)}+\cos\phi_6^{(3)}+\sin\phi_7^{(4)}-\sin\phi_8^{(4)})=0,\\ y: &\sin\alpha(+\cos\phi_1^{(1)}+\cos\phi_2^{(1)}-\sin\phi_3^{(2)}-\sin\phi_4^{(2)}-\cos\phi_5^{(3)}-\cos\phi_6^{(3)}\\ &+\sin\phi_7^{(4)}+\sin\phi_8^{(4)})+\cos\alpha(+\sin\phi_1^{(1)}-\sin\phi_2^{(1)}+\cos\phi_3^{(2)}\\ &-\cos\phi_4^{(2)}-\sin\phi_5^{(3)}+\sin\phi_6^{(3)}-\cos\phi_7^{(4)}+\cos\phi_8^{(4)})=0. \end{aligned} \tag{8}$$

Therefore, we obtain the following condition of rotation for α in $(0, \pi/2)$ from Eq. (8):

$$\begin{cases} \phi_1^{(1)} = \phi_5^{(3)}, \phi_2^{(1)} = \phi_6^{(3)}, \phi_3^{(2)} = \phi_7^{(4)}, \phi_4^{(2)} = \phi_8^{(4)}, & \forall\alpha, \\ \phi_1^{(1)} + \phi_8^{(4)} = \phi_4^{(2)} + \phi_5^{(3)}, \phi_2^{(1)} + \phi_3^{(2)} = \phi_6^{(3)} + \phi_7^{(4)}, & \alpha = \pi/4. \end{cases} \tag{9}$$

In a similar way for Eq. (5), we assume that all of the rotation parameters $\phi_j^{(i)}$ should be either +1 or −1 to take account of the necessary condition for the possible motion of a 4RE-linkage with a single degree of freedom. Based on this assumption, we let $\phi_1^{(1)} = +1$ and obtain the eight different modes, which are

$$\begin{aligned} &\{\phi_1^{(1)}\phi_2^{(1)}\phi_3^{(2)}\phi_4^{(2)}\phi_5^{(3)}\phi_6^{(3)}\phi_7^{(4)}\phi_8^{(4)}\} \\ &= \begin{cases} \{+1+1+1+1+1+1+1+1\}, & \forall\alpha, \\ \{+1+1-1-1+1+1-1-1\}, & \forall\alpha, \\ \{+1-1-1+1+1-1-1+1\}, & \forall\alpha, \\ \{+1-1+1-1+1-1+1-1\}, & \forall\alpha, \\ \{+1-1-1-1+1-1-1-1\}, & \forall\alpha, \\ \{+1-1+1+1-1-1+1-1\}, & \alpha = \pi/4. \\ \{+1-1+1+1-1+1-1-1\}, & \alpha = \pi/4. \\ \{+1-1+1+1+1+1-1+1\}, & \alpha = \pi/4. \end{cases} \end{aligned} \tag{10}$$

The rotational modes of Eq. (10) represent the basic motions of a 4RE-linkage, and indicate the ways the 4-bar joints connect to realize such motions. In other words, the 4RE-linkage can perform these motions only by being adequately connected at the joints. The structures of 4RE-linkages are determined by selecting the modes of connection based on Eq. (10); e.g., some of the 4RE-linkages are equivalent to the subtypes of closed double chain linkages consisting of four pairs of scissor-like elements (Mao et al., 2009). We now focus on the modes of connecting the joints and discuss about how to assemble the 4RE-linkages as a basic structural unit to clarify the characteristics of the motions defined by Eq. (10).

2.2. Repetitive assemblies of 4RE-linkages

Similar to a jigsaw puzzle, it is difficult to derive all of the motion patterns for a number of possible mobile assemblies, even though such motion patterns are formed by the minimum movable unit of the 4RE-linkages. In this section, we present certain types of repetitive and combined assemblies of 4RE-linkages, ranging from well-known to novel structures. We define a repetitive assembly as a structure built using only the identical rotational mode of the 8-bar joints, while a combined assembly stands for a structure built of multiple rotational modes.

Considering the finite number of repetitive assemblies of 4RE-linkages, we start by focusing on the 4RE-linkage in Fig. 2(a). Note that the motion conditions of Eq. (4) are $\theta_A = \theta_C$ and $\theta_B = \theta_D$, and the parameters for the 4RE-linkages have the relationships:

$$\begin{aligned} &\{\phi_1^{(1)}\phi_2^{(1)}\phi_3^{(1)}\phi_4^{(1)}\phi_5^{(3)}\phi_6^{(3)}\phi_7^{(3)}\phi_8^{(3)}\}, \\ &= \{\phi_5^{(2)}\phi_6^{(2)}\phi_7^{(4)}\phi_8^{(4)}\phi_1^{(4)}\phi_2^{(4)}\phi_3^{(2)}\phi_4^{(2)}\}. \end{aligned} \tag{11}$$

As shown in Fig. 3(a), we assume that the 4RE-linkages are assembled in a repetitive manner so that joint 1 of one unit corresponds to joint 3 of an adjacent unit and joint 2 corresponds to joint 4 of an adjacent unit. If each joint displays a coordinated rotation with a single degree of freedom, the motion of each 4RE-linkage is equivalent to the rotation of each 8-bar joint, which is indicated by replacing the superscripts of Eq. (11) with $3 \equiv 1$ and $4 \equiv 2$. Thus, using the parameters $\boldsymbol{\phi}^{(i_x,i_y)}$ illustrated in Fig. 3(b), the motion of these repetitive assemblies can be represented by the rotations of 8-bar joints arranged in a periodic square pattern, which are

$$\begin{aligned} &(n_x + n_y = 2p) : \boldsymbol{\phi}^{(i_x+n_x,i_y+n_y)} \\ &\quad = \left\{\phi_1^{(i_x,i_y)}\phi_2^{(i_x,i_y)}\phi_3^{(i_x,i_y)}\phi_4^{(i_x,i_y)}\phi_5^{(i_x,i_y)}\phi_6^{(i_x,i_y)}\phi_7^{(i_x,i_y)}\phi_8^{(i_x,i_y)}\right\} \end{aligned} \tag{12}$$

and

$$\begin{aligned} &(n_x + n_y = 2p+1) : \boldsymbol{\phi}^{(i_x+n_x,i_y+n_y)} \\ &\quad = \left\{\phi_5^{(i_x,i_y)}\phi_6^{(i_x,i_y)}\phi_7^{(i_x,i_y)}\phi_8^{(i_x,i_y)}\phi_1^{(i_x,i_y)}\phi_2^{(i_x,i_y)}\phi_3^{(i_x,i_y)}\phi_4^{(i_x,i_y)}\right\}, \end{aligned} \tag{13}$$

where n_x, n_y and p are integers. Therefore, by replacing Eq. (10) with the rotational modes of an 8-bar joint, the motions of the repetitive assemblies can be rewritten as

$$\begin{aligned} \boldsymbol{\phi}_0 &= \{+1+1+1+1+1+1+1+1\}, & \forall\alpha, \\ \boldsymbol{\phi}_1 &= \{+1+1-1-1+1+1-1-1\}, & \forall\alpha, \\ \boldsymbol{\phi}_2 &= \{+1-1-1+1+1-1-1+1\}, & \forall\alpha, \\ \boldsymbol{\phi}_3 &= \{+1-1+1-1+1-1+1-1\}, & \forall\alpha, \\ \boldsymbol{\phi}_4 &= \{+1-1-1-1+1-1-1-1\}, & \forall\alpha, \\ \boldsymbol{\phi}_5 &= \{+1-1+1-1-1-1+1+1\}, & \alpha = \pi/4, \\ \boldsymbol{\phi}_6 &= \{+1-1-1-1-1+1+1+1\}, & \alpha = \pi/4, \\ \boldsymbol{\phi}_7 &= \{+1-1-1+1+1+1+1+1\}, & \alpha = \pi/4, \end{aligned} \tag{14}$$

where $\boldsymbol{\phi}_k$ is serially numbered by $k = 0, \ldots, 7$. It is clear that the mismatch of the overall conformation never occurs under each motion of $\boldsymbol{\phi}_k$ because the transformation of each 4RE-linkage in the repetitive assemblies follows the condition of Eq. (9).

Eq. (14) only represent the possible motions of the 4RE-linkages. In fact, to realize these derived motions, we select the proper connection of an 8-bar joint, which corresponds to each rotational mode of Eq. (14). We then need to confirm whether the repetitive assemblies composed of the well-defined 8-bar joints can exhibit the motion behaviour with a single degree of freedom. Following the connection rule of an 8-bar joint, it is obvious for each $\boldsymbol{\phi}_k$ that all the bars with the same direction of rotation are rigidly connected together and all the bars with a different direction of rotation are pivotally connected together. Then, the rigid body coupled with bars can be counted as a single component under the Kutzbach criterion. For instance, in the case of $\boldsymbol{\phi}_3$, the rigid component formed by the odd-numbered bars and the rigid component formed by the even-numbered bars are hinged to each other as an 8-bar joint with $n = 2$ and $j_1 = 1$. According to the above method of connecting, 4RE-linkages can be repetitively assembled with identical joints. If the mechanism of the obtained repetitive assembly is greater than one ($m > 1$), the structure no longer has a single degree of freedom. On the other hand, the repetitive assembly with $m \leqslant 1$ can behave as a motion structure. In particular, it is not necessary for a motion structure with an overconstrained mechanism to have the entire number of 8-bar joints satisfying the connection rule to achieve motion.

Each mode $\boldsymbol{\phi}_k$ in Eq. (14) is discussed here. We define the motion of the repetitive assembly by $\beta\boldsymbol{\phi}_k$, where β indicates the coordinated rotation angle of all the beam members. The paths described by the movement of $\beta\boldsymbol{\phi}_k (k = 1, \cdots, 4)$ for 2×2 unit cells with $\alpha = 50^\circ$ are illustrated in Fig. 4, and the paths described by the movement of $\beta\boldsymbol{\phi}_k$ $(k = 5, 6, 7)$ for 2×2 unit cells with $\alpha = 45^\circ$ are illustrated in Fig. 5. The observations on each motion of the repetitive assemblies in Figs. 4 and 5 are summarized as follows:

(i) $k = 1$. The rotation of all the REs (indicated by the angle of the broken lines) constitutes the motion of $\boldsymbol{\phi}_1$ (Fig. 4(b)). This is one of the common modes of motion of square grids connected with scissor type revolute joints. Note that $m = -3$ from $n = 6$ and $j_1 = 9$ under the Kutzbach criterion. Therefore, this is overconstrained.

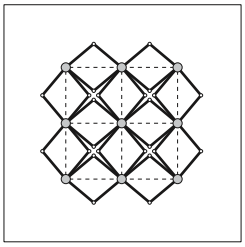

(a) initial configuration for $\alpha = 50^\circ$

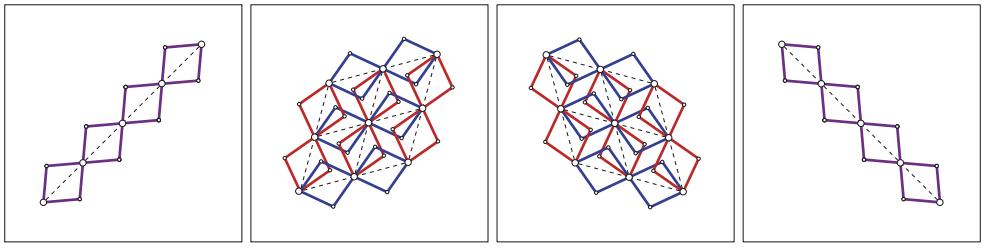

(b) The shapes of $\boldsymbol{\phi}_1 = \{+1\ +1\ -1\ -1\ +1\ +1\ -1\ -1\}$, rotated by $\beta = -45^\circ$, -15°, $+15^\circ$, $+45^\circ$ from left.

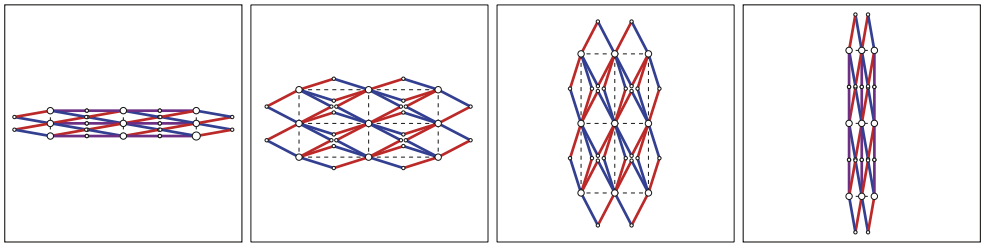

(c) The shapes of $\boldsymbol{\phi}_2 = \{+1\ -1\ -1\ +1\ +1\ -1\ -1\ +1\}$, rotated by $\beta = -40^\circ$, -22.5°, $+22.5^\circ$, $+40^\circ$ from left.

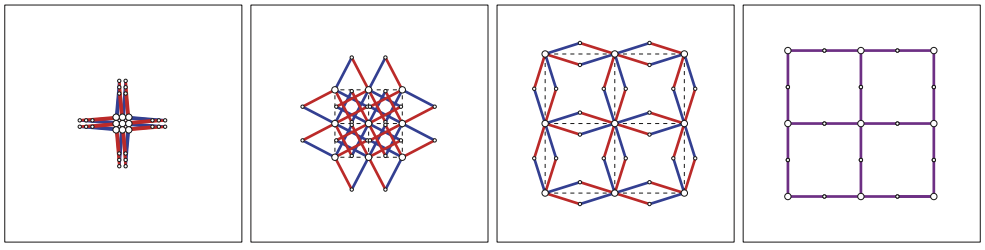

(d) The shapes of $\boldsymbol{\phi}_3 = \{+1\ -1\ +1\ -1\ +1\ -1\ +1\ -1\}$, rotated by $\beta = -45^\circ$, -22.5°, $+22.5^\circ$, $+40^\circ$ from left.

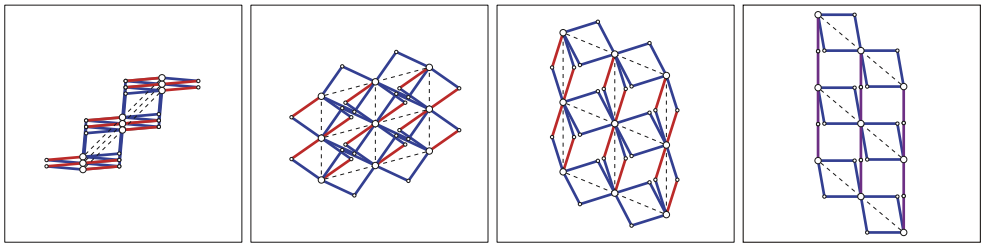

(e) The shapes of $\boldsymbol{\phi}_4 = \{+1\ -1\ -1\ -1\ +1\ -1\ -1\ -1\}$, rotated by $\beta = -45^\circ$, -15°, $+22.5^\circ$, $+40^\circ$ from left.

Fig. 4. Diagrams of the transformation of $\beta\boldsymbol{\phi}_k (k = 1, \ldots, 4)$ for $\alpha = 50^\circ$. Here, the red-colored bars exhibit the positive rotations and the blue-colored bars exhibit the negative rotations for each obtained mode. In addition, the purple-colored bars represent complete overlaps between the red-colored and blue-colored bars. The adjacent beam members painted in the same color, blue or red, are rigidly connected together on all the pivot joints. (For interpretation of the references to colour in this figure legend, the reader is referred to the web version of this article.)

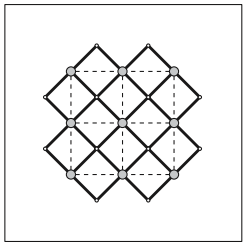

(a) initial configuration for $\alpha = 45°$

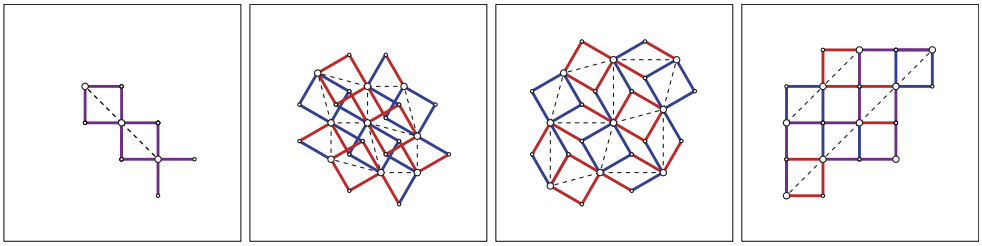

(b) The shapes of $\boldsymbol{\phi}_5 = \{+1\ -1\ +1\ -1\ -1\ -1\ +1\ +1\}$, rotated by $\beta = -45°$, $-15°$, $+15°$, $+45°$ from left.

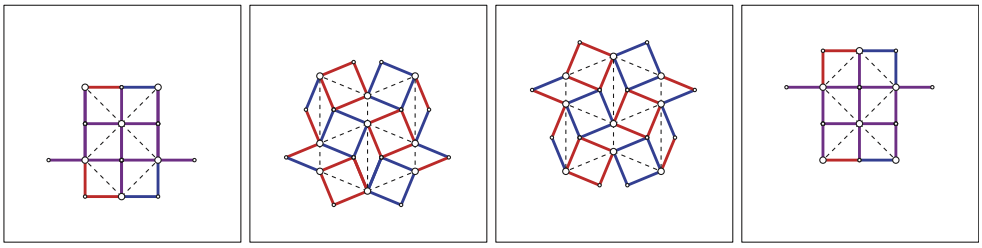

(c) The shapes of $\boldsymbol{\phi}_6 = \{+1\ -1\ -1\ -1\ -1\ +1\ +1\ +1\}$, rotated by $\beta = -45°$, $-22.5°$, $+22.5°$, $+45°$ from left.

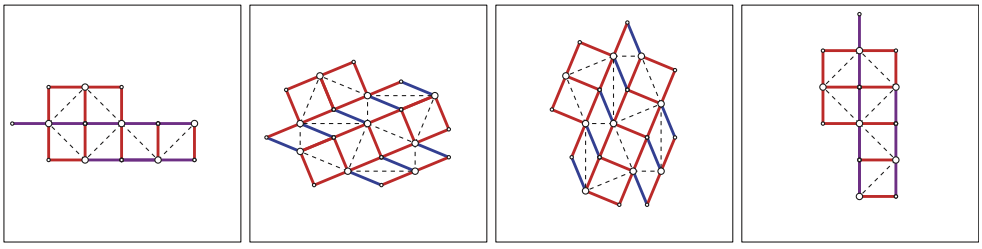

(d) The shapes of $\boldsymbol{\phi}_7 = \{+1\ -1\ -1\ +1\ +1\ +1\ +1\ +1\}$, rotated by $\beta = -45°$, $-22.5°$, $+22.5°$, $+45°$ from left.

Fig. 5. Diagrams of the transformation of $\beta\boldsymbol{\phi}_k (k = 5, 6, 7)$ for $\alpha = 45°$. The colors of the bars have the same meanings as the colors adopted in Fig. 4.

(ii) $k = 2$ and $k = 3$. The motions of $\boldsymbol{\phi}_2$ and $\boldsymbol{\phi}_3$ are made up entirely of transformations of REs, which accompany the elongation and contraction of the broken lines (Fig. 4(c) and (d)). These two structures are repetitively assembled with closed double chain linkages consisting of four pairs of scissor-like elements (Mao et al., 2009). The motion of $\boldsymbol{\phi}_2$ is nearly equal to the transformation of square grids with scissor hinges. It is apparent that the two motions of $\boldsymbol{\phi}_2$ and the square grids are completely consistent in the case of the initial configuration for $\alpha = \pi/4$. Meanwhile, the motion of $\boldsymbol{\phi}_3$ displays the overall contraction ($\beta < 0$) and expansion ($\beta > 0$) according to the similarity transformation of the regular squares enclosed by the broken lines. This motion is asymmetric to the rotational direction of β. Note that the two types of motion, both $\boldsymbol{\phi}_2$ and $\boldsymbol{\phi}_3$, are highly overconstrained mechanisms because $m = -15$ from $n = 18$ and $j_1 = 33$.

(iii) $k = 4$ and $k = 5$. Both motions of $\boldsymbol{\phi}_4$ and $\boldsymbol{\phi}_5$ are evenly mixed by the rotation and transformation of REs, and these shapes of the two motions display an asymmetrical relationship with respect to β; in other words, the structures expand with increasing β (Fig. 4(e) and Fig. 5(b)). In particular, in the case of the configurations for $\alpha = \pi/4$, the overall transformations change from two regular squares (minimum size) to 10 regular squares (maximum size) for both motions. Viewing the rotation of a RE as the angle of a broken line, each joint seems to be a 6-bar joint. Calculating the condition of the Kutzbach criterion for 6-bar joints gives $m = -9$ from $n = 12, j_1 = 21$.

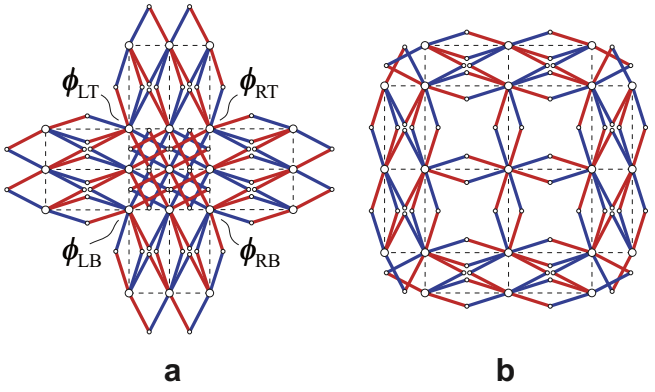

Fig. 6. The motion structure of the combined assembly with $\alpha = 50^\circ$ is made up of the rotational modes, ϕ_2, ϕ_3 and $\phi_{RT,LT,LB,RB}$: the conformation rotated by (a) $\beta = -22.5^\circ$ and (b) $\beta = +22.5^\circ$. The colors of the bars have the same meanings as the colors adopted in Fig. 4.

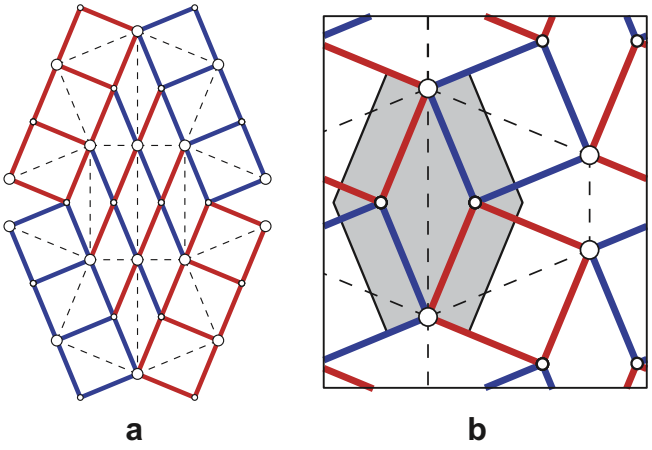

Fig. 7. (a) The motion structure of the combined assembly with $\alpha = 45^\circ$ is made up of the rotational modes, ϕ_2, ϕ_6 and ϕ_7; (b) The motion structure of (a) can become a shadow part of the repetitive assembly with only the rotational modes ϕ_6. The colors of the bars have the same meanings as the colors adopted in Fig. 4.

(iv) $k = 6$ and $k = 7$. Like ϕ_4 and ϕ_5, the motions of ϕ_6 and ϕ_7 are also evenly formed rotations and transformations of the REs, but both shapes of the two motions display a symmetrical relationship with respect to β (Fig. 5(c) and (d)). While moving, the number of connections on each joint is constantly four. Thus, these two motions can be classified as the transformations of square grids: in one, the adjacent regular square-blocks rotate in opposite directions (ϕ_6), and in the other, the in-line regular square-blocks rotate in the same direction (ϕ_7). The motion ϕ_6 shows that $m = -3$ from $n = 14, j_1 = 21$, which is consistent with the auxetic behaviour from rotating squares that is discussed by Grima and Evans (2000). On the other hand, the motion ϕ_7 shows that $m = 2$ from $n = 7, j_1 = 8$. Therefore, this conformation has two degrees of freedom. Fig. 5(d) shows the one-way transfer of rhombic transformation because of the orientation of the rotational mode ϕ_7. Because there are two lines of transfer in 2×2 cells, it is impossible to activate the motion of ϕ_7 by a single internal actuation.

We now propose the combined assemblies be built from 4RE-linkages with several different rotational modes obtained from Eq. (14). There are three kinds of combined assemblies described as structural examples in this study.

Fig. 6(a) and (b) show the first example of the structure, which is formed by the two types of motions of 4RE-linkages activated by ϕ_2 and ϕ_3 (Fig. 4(c) and (d)). Note that the rotational modes of the 8-bar joint on its four corners never conform to any part of Eq. (14). These modes, $\phi_{RT}, \phi_{LT}, \phi_{LB}, \phi_{RB}$, are respectively written as

$$\begin{aligned}
\phi_{RT} &= \{-1+1+1-1+1-1-1+1\},\\
\phi_{LT} &= \{-1+1-1+1+1-1+1-1\} = T(r^2)\phi_{RT},\\
\phi_{LB} &= \{+1-1-1+1-1+1+1-1\} = T(r^4)\phi_{RT},\\
\phi_{RB} &= \{+1-1+1-1-1+1-1+1\} = T(r^6)\phi_{RT},
\end{aligned} \tag{15}$$

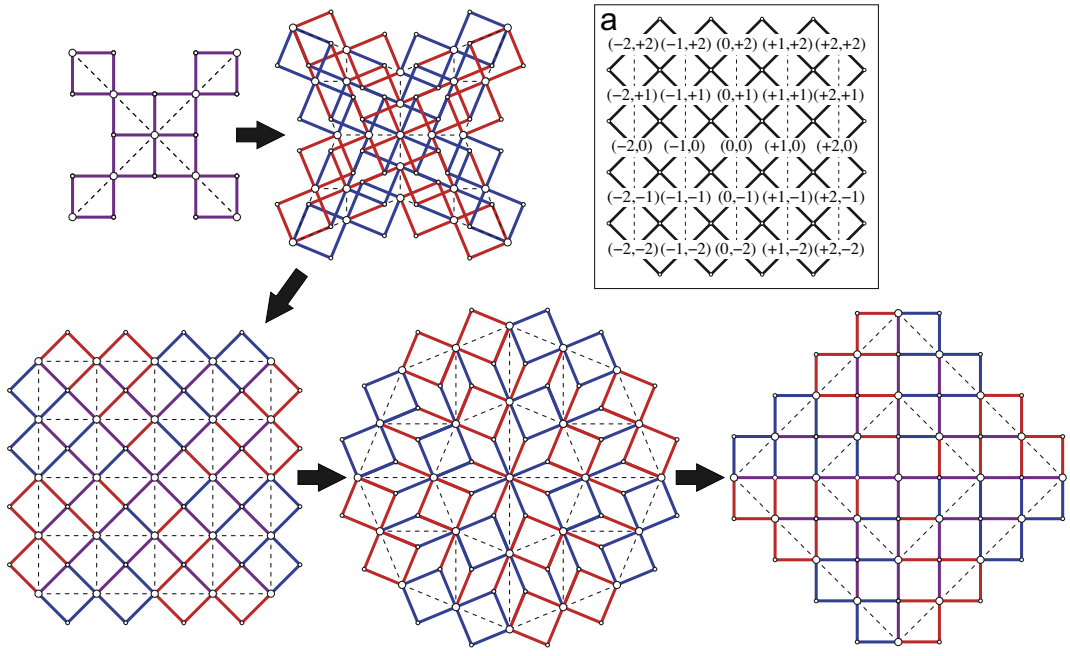

Fig. 8. The motion structure of the combined assembly with $\alpha = 45^\circ$ is made up of the rotational modes in Eq. (16): (a) shows the location index of each joint. The colors of the bars have the same meanings as the colors adopted in Fig. 4.

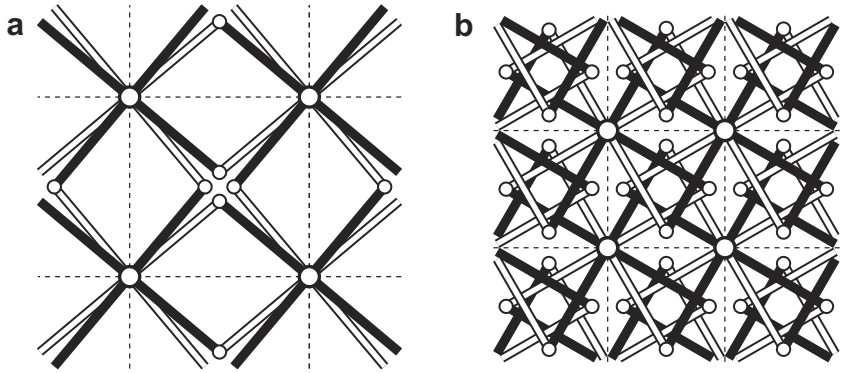

Fig. 9. Illustrations of the interference between components: (a) $\tan(\alpha+\beta)\approx 1$; (b) $\tan(\alpha+\beta)\approx 1/2$.

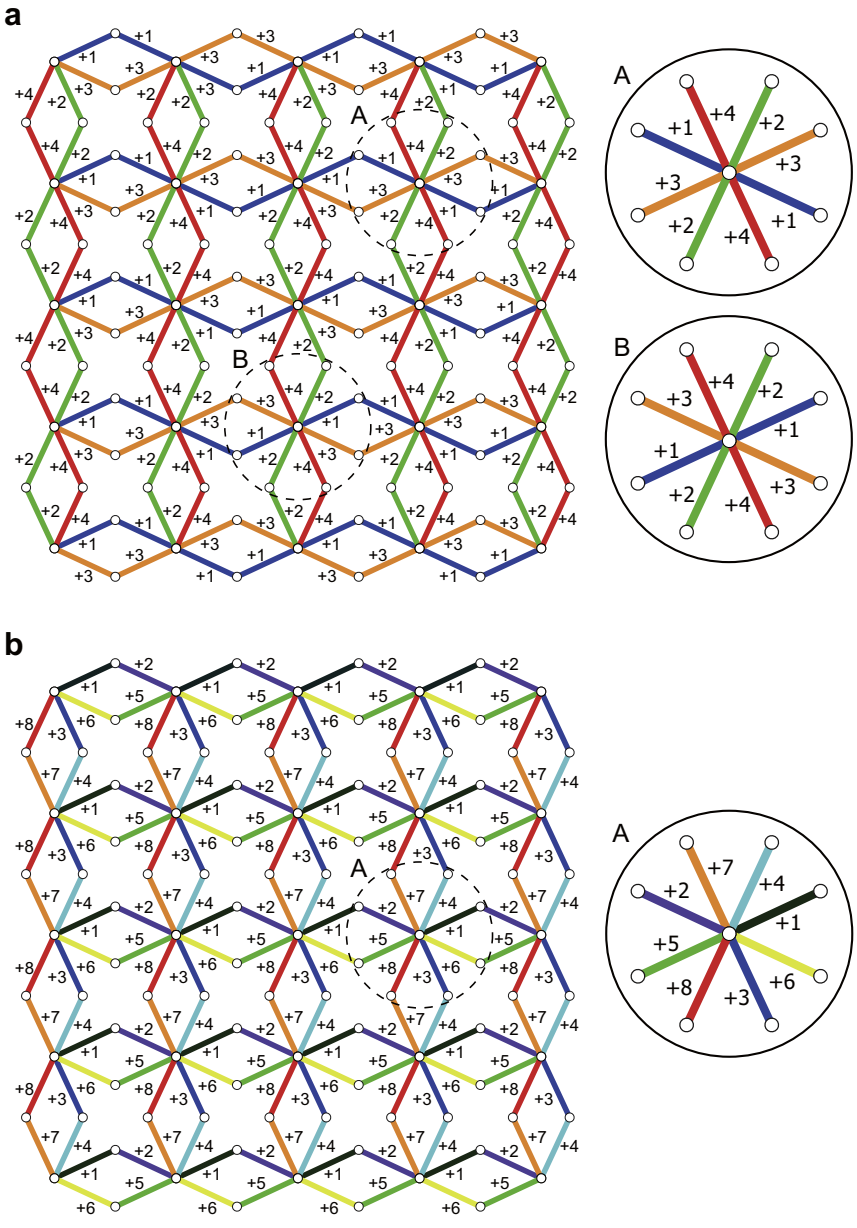

Fig. 10. Periodical patterns of the story levels in the repetitive assembly with ϕ_3: (a) 4 layers; (b) 8 layers.

where the operation of $T(r^q)$ transforms q-eighths of the circuit for the vector parameter $\boldsymbol{\phi}_{RT}$. The structure exists regardless of any initial configuration determined by α because two motions, both $\boldsymbol{\phi}_2$ and $\boldsymbol{\phi}_3$, are possible for an arbitrary α.

Second is the example of an assembly realized only for $\alpha = \pi/4$, as shown in Fig. 7(a) and (b). Fig. 7(a) shows that three rotational modes of $\boldsymbol{\phi}_2, \boldsymbol{\phi}_6$ and $\boldsymbol{\phi}_7$ constitute the motion. Moreover, as shown in Fig. 7(b), the arranged assemblies can make up an overall motion that is similar to the transformation mode of $\boldsymbol{\phi}_6$. Although it is a conventional motion resulting from square grids, the second example suggests that the combined motion with $\boldsymbol{\phi}_2, \boldsymbol{\phi}_6$ and $\boldsymbol{\phi}_7$ enables the structure to represent parts of the other motion, which correspond to the rotation and transformation of REs.

We also introduce one of the second type of combined assemblies as shown in Fig. 8. Considering the configuration of joints shown in the inset in Fig. 8(a), the rotational modes on joints are given as follows:

$$
\begin{aligned}
&\boldsymbol{\phi}^{(0,0)} = \boldsymbol{\phi}_3, \\
&\boldsymbol{\phi}^{(-1,+2)} = -T(r^1)\boldsymbol{\phi}_4, && \boldsymbol{\phi}^{(-2,+1)} = +T(r^2)\boldsymbol{\phi}_4, \\
&\boldsymbol{\phi}^{(-2,-1)} = -T(r^3)\boldsymbol{\phi}_4, && \boldsymbol{\phi}^{(-1,-2)} = +T(r^4)\boldsymbol{\phi}_4, \\
&\boldsymbol{\phi}^{(+1,-2)} = -T(r^5)\boldsymbol{\phi}_4, && \boldsymbol{\phi}^{(+2,-1)} = +T(r^6)\boldsymbol{\phi}_4, \\
&\boldsymbol{\phi}^{(+2,+1)} = -T(r^7)\boldsymbol{\phi}_4, && \boldsymbol{\phi}^{(+1,+2)} = +T(r^0)\boldsymbol{\phi}_4, \\
&\boldsymbol{\phi}^{(-1,+1)} = \boldsymbol{\phi}^{(-2,+2)} = +T(r^0)\boldsymbol{\phi}_5, && \boldsymbol{\phi}^{(-1,0)} = \boldsymbol{\phi}^{(-2,0)} = -T(r^1)\boldsymbol{\phi}_5, \\
&\boldsymbol{\phi}^{(-1,-1)} = \boldsymbol{\phi}^{(-2,-2)} = +T(r^2)\boldsymbol{\phi}_5, && \boldsymbol{\phi}^{(0,-1)} = \boldsymbol{\phi}^{(0,-2)} = -T(r^3)\boldsymbol{\phi}_5, \\
&\boldsymbol{\phi}^{(+1,-1)} = \boldsymbol{\phi}^{(+2,-2)} = +T(r^4)\boldsymbol{\phi}_5, && \boldsymbol{\phi}^{(+1,0)} = \boldsymbol{\phi}^{(+2,0)} = -T(r^5)\boldsymbol{\phi}_5, \\
&\boldsymbol{\phi}^{(+1,+1)} = \boldsymbol{\phi}^{(+2,+2)} = +T(r^6)\boldsymbol{\phi}_5, && \boldsymbol{\phi}^{(+1,0)} = \boldsymbol{\phi}^{(+2,0)} = -T(r^7)\boldsymbol{\phi}_5.
\end{aligned}
\tag{16}
$$

According to the given rotational modes of Eq. (16), the proposed structure transforms while maintaining high symmetry as shown in Fig. 8. In particular, the motion activated by $\beta = 0^\circ$ to 45° achieves the quarter rotation of the overall square cells through the configuration with D_8 symmetry, which has an 8-fold rotation centre and 8 axes of symmetry passing through the centre (Coxeter, 1961).

3. Manufactured model

In Section 2, some possible motions of 4RE-linkages have been derived without considering whether the straight bars and joints might make contact during motion. In fact most of the obtained planar motions interfere in this manner, e.g., $\boldsymbol{\phi}_3$ and $\boldsymbol{\phi}_4$ (Fig. 4(c) and (d)). In this section, we assume the repetitive assembly with $\boldsymbol{\phi}_3$ and make a physical model of the motion structure to determine actual conformations that overcome the above problem.

The planar motion of a repetitive assembly with $\boldsymbol{\phi}_3$ exhibits periodicity with D_4 symmetry on each unit cell. In the folding process, the first contact of their components may occur on each unit for $\alpha + \beta = 45^\circ$ (see Fig. 9(a)). After that, the contacts between the components of different cells are repeated up to a minimum size for $\alpha + \beta = 0^\circ$. For example, Fig. 9(b) illustrates the motion state just before the secondary contacts on the cell lines. Therefore, it is necessary for each module to assemble the bars and joints at an appropriate height to avoid contacts when applying the rule of periodicity. To address the above problem, there are two examples of assemblies with hierarchical modules shown in Fig. 10(a) and (b). Here, the height levels are numbered, with the lowest level starting at +1.

The former structure is assembled by applying two types of module in 4 layers. One module corresponds to the inset of circle A and the other module corresponds to circle B (Fig. 10(a)). In the case of circle A, two rigid cross-bars blended at levels (+1,+2) and at levels (+3,+4) comprise the module. Similarly, in the case of circle B, two rigid cross-bars blended at level (+1,+4) and at level (+2,+3) comprise a module. In both cases, the two types of modules are made up of their two rigid cross-bars connected by pivots. This type of structure shown in Fig. 10(a) was first described in Hoberman Designs Inc. (2011).

The latter structure is simply assembled using a single type of module with 8 layers (Fig. 10(b)). However, unlike the modules with 4 layers, the rotational mode $\boldsymbol{\phi}_3$ of the module with 8 layers cannot be achieved with only a simple pivot. To realize the rotational mode $\boldsymbol{\phi}_3$ of the module with 8 layers, it is necessary to

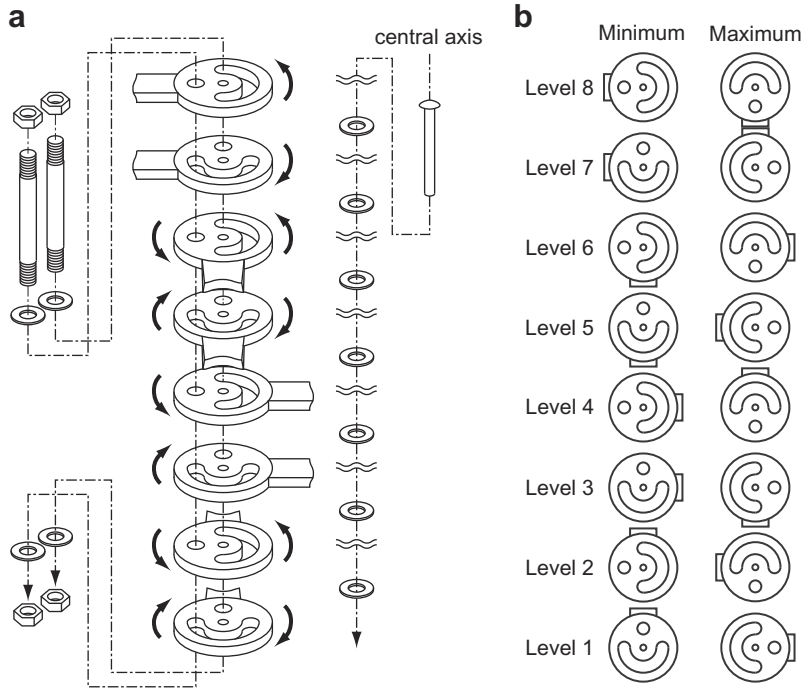

Fig. 11. (a) Exploded view of the designed 8-bar joint; (b) the configurations of the disc-joints for the minimum contraction and maximum expansion states of the repetitive assembly with $\boldsymbol{\phi}_3$.

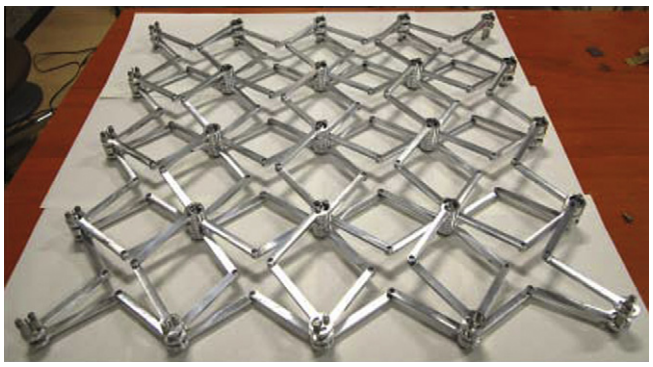

Fig. 12. Overview of a manufactured repetitive assembly with ϕ_3 (4×4 cells).

connect the two cross-bars with pivots, each of which is rigidly jointed by the bars at levels (+1, +3, +5, +7) or the bars at levels (+2, +4, +6, +8), respectively. Fig. 11(a) illustrates an exploded view of the module with 8 layers, which is a design proposal that enables a rotational mode ϕ_3. For this module, eight bars with disc-joints are stacked by centering on a pin. Each disc-joint has a small hole in the centre to accommodate the location pin, and a circle hole and a circular arc hole, which are located on the concyclic line. Then, two identical stud-bolts pass through either the circle hole or the circular arc hole of each disc-joint. One stud-bolt is inserted into the circle holes of the disc-joints at levels (+1, +3, +5, +7) and the circular arc hole of the disc-joints at levels (+2, +4, +6, +8), and vice versa. Because the stud-bolts through the circle holes are fixed and the stud-bolts through the circular arc holes can freely rotate in the plane of the disc-joints, the design module satisfies the connective condition for ϕ_3 as mentioned above. For instance, Fig. 11(b) shows the configuration of the disc-joints at each level as the minimum size ($\alpha + \beta = 0^\circ$) and the maximum size ($\alpha + \beta = 90^\circ$) of the structure.

Fig. 12 shows the manufactured structure made up of modules with 8 layers. The structure forms 4×4 cells and its modules are connected by revolute joints as 2-bar joints. Note that the modules on the boundary consist of the minimum number of bars for the connections. The solid bar, integrated with a disc-joint, is made from aluminum. Each bar ℓ is 100 mm long, and the total weight of the structure is about 2.4 kg.

As shown in Fig. 13(a)–(d), the expanding motion of the manufactured structure is driven by a single rotary actuator acting on the centre module, the position of which is (0,0). The minimum size of the manufactured model is 320×320 mm^2, and the maximum size is 830×830 mm^2. The deployment rate is about 2.6. Note that the four modules on $(\pm 1, \pm 1)$ are suspended from the ceiling to avoid increasing the friction in the joints and bars because of the deflection of the overall structure. For the centre module, the disc-joints at levels (+2,+4,+6,+8) are fixed on the ground and the disc-joints at levels (+1,+3,+5,+7) are rotated clockwise by the actuation. Therefore, the expanding motion of this system is

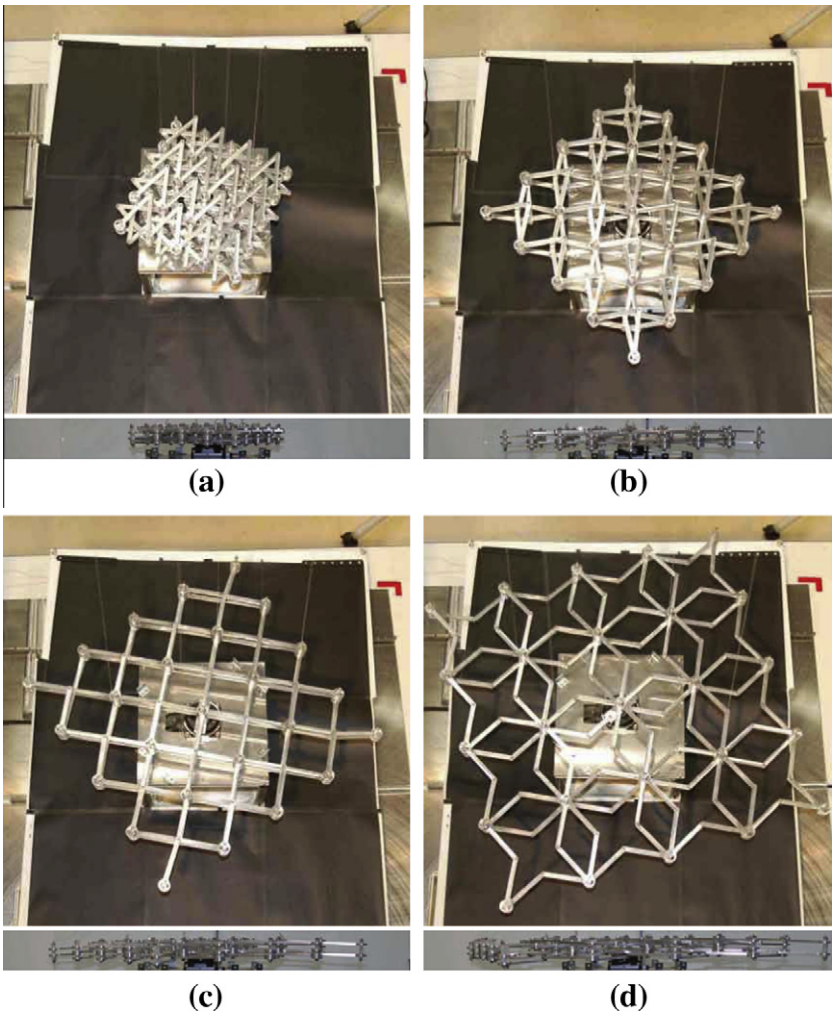

Fig. 13. Top and side photographs of the expanding behaviour of the repetitive assembly with ϕ_3. A sequence of expanding and folding motions is available as Supplementary Movie S1.

the mixture mode of ϕ_0 and ϕ_3. Both modes are invertible. Hence, the folding motion with ϕ_0 and ϕ_3 can be driven by reversed rotation of the actuator. For the shape in Fig. 13(c), it can be seen that this motion structure has a kinematic bifurcation point with respect to the modules located on the four corners. This is not significant for the overall motion because each secondary path immediately recovers the primary path in real motion (Supplementary Movie S1).

4. Conclusions

We have demonstrated seven types of motion pattern for a 4RE-linkage by straightforward calculations based on geometric considerations, and have also proposed certain motions of the repetitive assemblies to select the combinations of the obtained motions for a 4RE-linkage. To produce a highly symmetric structure with D_4 symmetry, we have examined a variety of telescopic motions, which range from those based on the well-known behaviour of square grids to novel mobility modes that are not yet publically available. In particular, the combined motion in Fig. 8 is interesting from the point of view of structural mechanics. This movable structure potentially has high stiffness with D_8 symmetry if it can be made to transform to the bidirectional square grids (0°- or 45°-axial direction) in response to changing external loads.

In addition, we have manufactured a repetitive assembly built out of modules that have foldable and expandable motion resulting from the rotational mode ϕ_3 of the 8-bar joints. To avoid interference between the components, we have developed a hierarchical framework connected by modules with 8 layers, each of which enables the rotation of ϕ_3. In fact, a deployable motion has been demonstrated resulting from the coordinated motions of all the modules, which are internally activated by a single rotary actuation.

Through this work, we have introduced certain rotational modes of an 8-bar joint, which determine the transformation of the motion structure assembled with 4RE-linkages. The complexity of the joint as observed in the manufactured test structure seems to be undesirable for a mechanical system. However, a structural concept that focuses on the rotational modes of connections might become a key item for developing novel spatial structures in two- and three-dimensional solids.

For instance, Verheyen (1989a) developed a complete set of three-dimensional spatial structures with polyhedron motions based on the *Jitterbug* transformation (Fuller, 1975). In the one of Verheyen's architectures, the cubic structure is made up of dipolygon units in each of which two square plates are connected by a pinned joint passing through the centres of the squares (Verheyn, 1989b). It can be observed that each planar motion of the Verheyen's cube is consistent with the rotational mode ϕ_3 of an 8-bar joint: in this way, the 4 half-diagonals of a square form 4 bars, and the two squares produce 8 bars meeting at the centre, forming an 8-bar joint. The above instance suggests that the two-dimensional structure with planar mobility can be used as three-dimensional space fillers that transform into other space fillers in each position. Thus, our proposed structures can be extended to general spatial structures when considering the projections of three-dimensional motions and their proper configurations.

Acknowledgements

The author (HT) gratefully acknowledges the financial support of the Japan Society for the Promotion of Science for Young Scientists (Grant Nos. 21860053 and 23760086).

Appendix A. Supplementary data

Supplementary data associated with this article can be found, in the online version, at http://dx.doi.org/10.1016/j.ijsolstr.2012.03.008.

References

Akgün, Y., Gantes, C.J., Kalochairetis, K.E., Kiper, G., 2010. A novel concept of convertible roofs with high transformability consisting of planar scissor-hinge structures. Engineering Structures 32, 2873–2883.
Ashby, M.F., 1992. Materials Selection in Mechanical Design. Pergamon Press, Oxford, UK.
Buhl, T., Jensen, F.V., Pellegrino, S., 2004. Shape optimization of cover plates for retractable roof structures. Computer & Structures 82, 1227–1236.
Calladine, C.R., 1978. Buckminster Fuller's Tensegrity structures and Clerk Maxwell's rules for the construction of stiff frames. International Journal of Solids and Structures 14, 162–172.
Coxeter, H.S.M., 1961. Introduction to Geometry. Wiley.
Deshpande, V.S., Ashby, M.F., Fleck, N.A., 2001. Foam topology bending versus stretching dominated architectures. Acta Materialia 49, 1035–1040.
Evans, K.E., Alderson, A., 2000. Auxetic materials: functional materials and structures from lateral thinking! Advanced Materials 12, 617–628.
Evans, K.E., Nkansah, M.A., Hutchinson, I.J., Rogers, S.C., 1991. Molecular network design. Nature 353, 124–125.
Fuller, R.B., 1975. Synergetics: Exploration in the Geometry of Thinking. Macmillan, New York.
Gaspar, N., Ren, X.J., Smith, C.W., Grima, J.N., Evans, K.E., 2005. Novel honeycombs with auxetic behaviour. Acta Materialia 53, 2439–2445.
Gibson, L.J., Ashby, M.F., 1997. Cellular Solids: Structural and Properties, second ed. Cambridge University Press, Cambridge.
Grima, J.N., Evans, K.E., 2000. Auxetic behavior from rotating squares. Journal of Materials Science Letters 19, 1563–1565.
Grübler, M., 1917. Getriebelehre. Springer, Berlin.
Guest, S.D., Fowler, P.W., 2005. A symmetry-extended mobility rule. Mechanism and Machine Theory 40, 1002–1014.
Hoberman, C., 1990. Reversibly expandable doubly-curved truss structure. US Patent 4,942,700.
Hoberman, C., 1991. Reversibly expansion/retraction truss structure. US Patent. 5,024,031.
Hoberman Designs, Inc., Hoberman Associates, Inc., 2011. 1680, 40 Worth Street. Suite, New York 10068, USA. <http://www.hoberman.com> (accessed 18.10.2011).
Hunt, K.H., 1978. Kinematic Geometry of Mechanisms. Clarendon Press, Oxford, UK.
Kumar, P., Pellegrino, S., 2000. Computation of kinematic paths and bifurcation points. International Journal of Solids and Structures 37, 7003–7027.
Kutzbach, K., 1929. Mechanische Leitungsverzweigung Maschinenbau. Der Betrieb 8, 710–716.
Lengyel, A., 2002. Analogy between equilibrium of structures and compatibility of mechanisms. PhD Thesis, University of Oxford.
Mao, D., Luo, Y., You, Z., 2009. Planar closed loop double chain linkages. Mechanism and Machine Theory 44, 850–859.
Patel, J., Ananthasuresh, G.K., 2007. A kinematic theory for radially foldable planar linkages. International Journal of Solids and Structures 44, 6279–6298.
Smith, C.W., Grima, J.N., Evans, K.E., 2000. A novel mechanism for generating auxetic behaviour in reticulated foams: missing rib foam model. Acta Materialia 48, 4349–4356.
Tanaka, H., Shibutani, Y., 2008. Large deformability of 2D framed structures connected by flexible joints. Journal of Solid Mechanics and Materials Engineering 2, 1037–1048.
Tanaka, H., Shibutani, Y., 2009. In-plane mechanical behaviors of 2D repetitive frameworks with four-coordinate flexible joints and elbowed beam members. Journal of the Mechanics and Physics of Solids 57, 1485–1499.
Tarnai, T., 2001. Kinematic bifurcation. In: Pellegrino, S. (Ed.), Deployable Structures CISM Courses and Lectures, vol. 412. Springer, Wien, New York, pp. 113–142 [Chapter 8].
Verheyen, H.F., 1989a. The complete set of Jitterbug transformers and the analysis of their motion. Computers & Mathematics with Applications 17, 203–250.
The cubic motion structure developed by Verheyn, H.F. can be found in Fig. 33 of Ref. VHF89a.
Wicks, N., Guest, S.D., 2004. Single member actuation in large repetitive truss structures. International Journal of Solids and Structures 41, 965–978.
You, Z., 1997. Foldable bar structures. International Journal of Solids and Structures 34, 1825–1847.
You, Z., 2007. Motion structures extend their reach. Materials Today 10, 52–57.